Monatsh Chem 139, 389–399 (2008)
DOI 10.1007/s00706-007-0779-y
Printed in The Netherlands

Monatshefte für Chemie
Chemical Monthly

First-principles approach to the understanding of π-conjugated organic semiconductors

Peter Puschnig, Claudia Ambrosch-Draxl

Lehrstuhl für Atomistic Modelling and Design of Materials, Department für Materialphysik, Montanuniversität Leoben, Leoben, Austria

Received 29 May 2007; Accepted 18 July 2007; Published online 14 March 2008
© Springer-Verlag 2008

Abstract We show how *ab initio* calculations based on density functional theory contribute to the understanding of the electronic and optical properties of organic semiconducting materials, which form the active layers in many opto-electronic applications. As a textbook example, we present the electronic structure and the optical properties of the oligo-phenylenes as evolving from their benzene-constituents. Thereby we discuss the dependence on the molecular length and introduce the modifications in the opto-electronic properties due to intermolecular interactions which are inherently present in the bulk phase.

Keywords *Ab initio* calculations; Electronic structure; Oligomers; Optical properties; Solid state.

Introduction

In organic semiconductor research, the focus of interest has been for a long time on polymers and their chemical functionalization in order to tune their opto-electronic properties, *e.g.*, the electroluminescence quantum yield, the charge carrier mobility, or the photoconductivity. A huge variety of conjugated homo-, block-, and co-polymers has been synthesized and investigated in terms of their suitability to operate as active materials in devices such as organic light emitting diodes (OLEDs) [1–3], organic thin-film transistors (OTFTs) [4], organic photovoltaic diodes (OPVDs) [5–7], or lasers [8, 9]. Among them, particularly those based on poly-acetylene, poly-*para*-phenylene (*PPP*), poly-*para*phenylene-vinylene (*PPV*), poly-thiophene, and poly-fluorene backbones [10, 11] have become prominent candidates for these applications. Apart from conducting polymers, organic materials consisting of small π-conjugated molecules, which form well defined molecular crystals, have attracted great attention over the last two decades. For example, an OLED has been realized with *para*-hexaphenyl [12], which exhibits remarkable optical properties. The polarization of its electroluminescence can be changed through the molecular alignment. Other examples are sexithiophene and pentacene, which have been successfully used in OTFTs [13–16].

Besides, the manifold of experimental investigations on electronic and optical properties [17, 18], a variety of theoretical methods have also been applied to both, polymers and oligomers. First, one has to distinguish between approaches dealing with isolated molecules as opposed to calculations for extended systems. The former has traditionally been the domain of quantum-chemical computations, which have proven to accurately characterize ground state

Corresponding: Peter Puschnig, Lehrstuhl für Atomistic Modelling and Design of Materials, Department für Materialphysik, Montanuniversität Leoben, Leoben, Austria. E-mail: peter.puschnig@mu-leoben.at

as well as excited state geometries and transition energies for isolated molecules. There have also been attempts to take into account the effects of the three-dimensional (3D) periodicity by using quantum chemical cluster approaches [19–21]. However, the unfavorable scaling of these *Hartree-Fock* based methods with the system size does not allow for a comprehensive treatment of the full 3D structure of real materials. On the other hand, approaches based on *ab initio* density functional theory (DFT) have the advantage that the full 3D crystal periodicity of the organic semiconductors can be easily taken into account. Indeed, the importance of intermolecular interactions on the electronic and optical properties has been proven for several materials including oligo-acenes [22–25], the oligo-phenylenes [26–28], and the phenylene-vinylenes [29]. In particular, band dispersions and splittings found in the oligo-acenes, for instance, are in good agreement with experimental findings [22–24], which highlights the necessity to consider the full 3D structure feasible in the framework of DFT.

In this review, we present a cross section of our *ab initio* approach to π-conjugated organic semiconductors carried out in our research group in the past decade, where the focus lies on the understanding of the basic physical phenomena. We start out with a short presentation of density functional theory, which forms the very basis of all theoretical results presented here, followed by a brief account on how to obtain optical properties from first principles. The main part of the paper is then devoted to the electronic and optical properties of the oligo-phenylenes in the bulk phase. This class of materials represents a prototype example for organic semiconductors composed of short π-conjugated molecules. It is shown how one can understand the electronic structure of the *isolated* molecule as evolving from its benzene-constituents. Thereby, the dependence of electro-optical properties on the molecular length will become evident. Most importantly, we will introduce the effect of *intermolecular* interactions which are inherently present in the bulk phase. We will discuss its consequences on the electronic band structure and the optical properties. The remainder of the paper concentrates on the nature of the optically excited state, *i.e.*, whether it is a free electron-hole state or a bound exciton, before we come to some conclusions and give an outlook to future projects.

Theoretical approach

Density functional theory

The fundamental theorem of *Hohenberg-Kohn* [30] states that the total energy of a system of interacting electrons is a functional of the electron density, and that the ground state density minimizes this functional resulting in the ground state energy. Formally, the *Hohenberg-Kohn* principle provides a strict relation for the ground state energy entirely in terms of the electron density distribution. In the formulation of *Kohn* and *Sham* [31] this minimizing density can be obtained by solving a single-particle *Schrödinger* equation with an effective potential, where the density is constructed from the corresponding auxiliary single particle orbitals. This is the so-called *Kohn-Sham* equation which has to be solved self-consistently, where the effective potential (*Kohn-Sham* potential) is defined as the sum of the external potential due to the atomic nuclei, the *Hartree*, and the exchange-correlation (xc) potential. The xc potential is obtained as the functional derivative of the exchange-correlation energy with respect to the electron density. Note that with the exact xc energy and potential all many-body effects are in principle included in the calculation of the ground state properties.

The simplest approximation to the xc functional is the so-called local-density approximation (LDA) in which the local contribution to the xc energy of the non-uniform system is taken to be identical to the xc energy of the uniform electron gas of the same density. It turned out that the LDA gives remarkably good results not only for free-electron like metals but also for atoms and molecules where the condition of slowly varying densities is not satisfied. Indeed, a large number of calculations have shown that the LDA values for structural properties such as bond lengths or vibrational frequencies agree within 1–5% when compared to experimental values [32, 33]. A more sophisticated expression for the exchange-correlation is the so-called generalized gradient approximation (GGA) [34] which has been shown to improve the description of structural properties for systems which considerably differ from the free-electron gas, such as molecules. Both types of functionals, however, do not include *van der Waals* (*vdW*) interactions and hence are not capable of predicting lattice parameters of organic semiconductors. In contrast, the internal, *i.e.*, the molecular geometry

as well as the electronic properties are not sensitive to the choice of the xc potential and are given reliably.

Optical properties

The linear optical response of a material to an external electric field is described by the complex dielectric function (*DF*), which is a tensor of 2nd rank for crystals with other than cubic symmetry. Following the pioneering work of *Adler* [35] and *Wiser* [36] who derived the linear response of periodic crystals within the so-called random phase approximation (RPA), the imaginary part of the dielectric tensor for a system with a band gap between occupied and unoccupied states is given by the sum over all interband transitions weighted by the momentum matrix elements [37]. Details on the theoretical as well as on computational aspects are outlined in a recent publication [38].

The RPA approach is derived within the so-called independent quasi-particle approximation in which the excited electron and the remaining hole are treated neglecting their *Coulomb* and exchange interaction. It is assumed that the quasi-particle correction to the *Kohn-Sham* eigenvalues can be accounted for by a constant, $\boldsymbol{k}$ independent correction Δ_c of the unoccupied conduction states (scissors operator). A review on *ab initio* techniques that go beyond the independent quasi-particle approximation and include excitonic effects by either solving the *Bethe-Salpeter* equation for the electron-hole correlation function or by making use of the time-dependent version of density functional theory can be found in Ref. [39]. The impact of excitonic effects on organic semiconductors is reviewed in Ref. [40].

Computational details

The numerical solution of the *Kohn-Sham* equation is commonly accomplished by expanding the *Kohn-Sham* orbitals into a suitable basis which transforms the problem into a generalized matrix eigenvalue problem, the so-called secular equation. The basis is chosen in a way to reflect the symmetry of the system under study. Hence, for crystals displaying translational symmetry the basis functions are *Bloch* waves. A special basis set is given by linearized augmented plane waves (LAPWs) which consist of plane waves in the interstitial region between the atoms and atomic-like functions close to the atomic nuclei. This construction allows for an all-electron treatment including core electrons without the need for simplifications in the potential and at the same time reduces the number of necessary basis function to about 100 per atom. Nevertheless, this restricts the evaluation of the *Kohn-Sham* equation to systems for which the crystal unit cell contains up to a few hundred atoms. We mention that all ground state calculations presented in this review have been carried out using the full-potential (linearized) augmented plane wave ((L)APW) plus local orbitals (lo) method as implemented in the WIEN2k code [41]. Computational details of our *ab initio* DFT approach for the calculation of organic molecular crystals are published elsewhere [27, 28].

Materials and crystal structures

In the gaseous state the oligo-phenylenes are non-planar molecules with alternating torsion angles between adjacent phenyl rings. This torsion angle ranges from 44° for biphenyl [42] to 30–40° for the longer oligomers [43]. The inter-ring torsion is the consequence of two competing forces. On the one hand, the π-electron system of the carbons at the inter-ring position tends to planarize the molecule, while on the other hand the electrostatic repulsion of the positively charged *ortho*-hydrogens on neighboring rings forces the molecule into a nonpla-

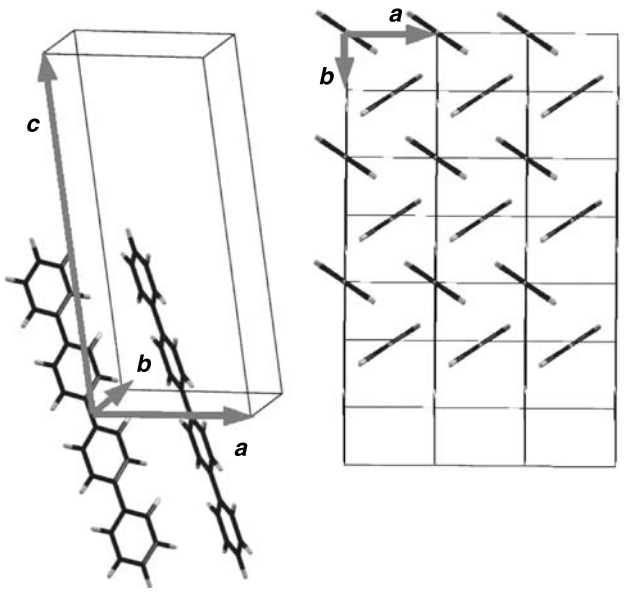

Fig. 1 The monoclinic unit cell of quaterphenyl containing two inequivalent molecules (left). The molecules form layers in the *ab*-plane leading to a so-called herring-bone arrangement (right). The lattice vectors $\boldsymbol{a}$, $\boldsymbol{b}$, and $\boldsymbol{c}$ are indicated by the arrows

Table 1 Experimental unit cell parameters for the oligophenylenes at room temperature for the monoclinic space group $P2_1/a$

Oligomer	a/Å	b/Å	c/Å	β/°
Biphenyl [45]	8.12	5.63	9.51	95.1
Terphenyl [46]	8.106	5.613	13.613	92.1
Quaterphenyl [47]	8.110	5.610	17.91	95.80
Hexaphenyl [48]	8.091	5.568	26.241	98.17

nar configuration. In the solid state we expect the interchain interactions packing forces to result in more planar molecules compared to the gas phase. For the infinite polymer, DFT calculations [26] have shown that the optimal inter-ring torsion angle is 18° which is in agreement with experiment [44]. For the oligomers, on the other hand, X-ray and neutron diffraction experiments at room temperature reveal a planar configuration of the molecules in the monoclinic space group $P2_1/a$ with two molecules per unit cell (see Fig. 1).

As exemplified for the case of quaterphenyl (*4P*), two phenyl rings set up the inequivalent atoms within one unit cell. The other half of the quaterphenyl molecule and the second molecule with its inversion center in the middle of the *ab* plane are generated by the inversion, screw axis and glide plane operations of the $P2_1/a$ space group. In Table 1, the experimental values for the lattice parameters a, b, c and the monoclinic angle β are given as obtained from single crystal X-ray diffraction. We observe that a and b remain almost constant as a function of the oligomer length. The very small reduction with increasing oligomer length indicates a slightly denser packing for longer molecules within the herring bone arrangement. The increase in c for longer oligomers is simply a consequence of the growing length of molecules which are approximately parallel to c.

Electronic structure

Dependence on molecular length

In order to understand the evolution of the electronic states of the oligo-phenylenes with increasing size we start out with a discussion of the molecular orbitals (MOs) of a single benzene ring. For instance, biphenyl is composed of two benzene rings as schematically depicted in Fig. 2a. Energetically, the π-orbitals constitute the highest occupied molecular orbital (HOMO) and the lowest unoccupied molecular orbital (LUMO). Benzene belongs to the D_{6h} point group, and, taking the six carbon π-orbitals as basis functions, the HOMO belongs to the e_{1g} irreducible representation of D_{6h}. The local symmetry of each of the benzene moieties in biphenyl changes from D_{6h} to C_{2v}. Thus, the doubly degenerate e_{1g} states are now split up into b_1 and a_2 states. Combining the two benzene moieties into biphenyl with D_{2h} symmetry results in the actual biphenyl MOs, for which the atomic orbital compositions of the highest four occupied MOs are displayed. The $1a_u$ and $1b_{1g}$ states of biphenyl, originating from the a_2 MOs of benzene, are close in energy, because the interaction across the inter-ring bridge is weak. These states are mainly *localized* at the benzene rings and are *non-bonding* with respect to the inter-ring bond. On the other hand, the interaction of the b_1 benzene states forming the $2b_{3u}$ and $2b_{2g}$ states of biphenyl is large, and so is their energetic separation. The corresponding wave functions are spread over the whole

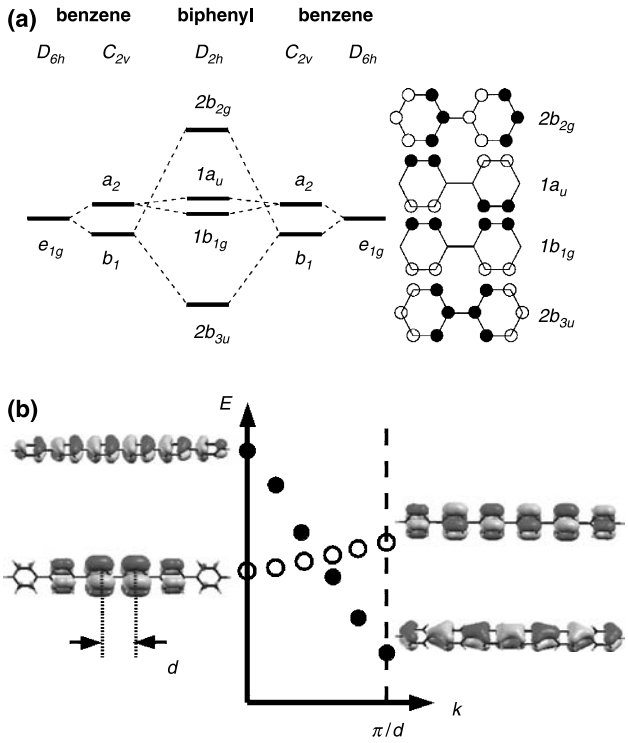

Fig. 2 (a) Diagram showing the evolution of the molecular orbitals of biphenyl from the MOs of two benzene rings. According to a *Hückel* picture, the atomic orbital compositions of the top four HOMOs are depicted. Filled (open) circles correspond to π-orbitals that have positive (negative) at one side of the molecular plane. (b) Molecular orbitals of the six-ring oligomer *para*-hexaphenyl. Filled (open) circles correspond to delocalized (localized) molecular orbitals

molecule (*delocalized* states) forming the inter-ring *bonding* ($2b_{3u}$) and *anti-bonding* ($2b_{2g}$) orbitals.

For the *n*-unit oligomer (*nP*) the *n* a_2 benzene MOs form *n* MOs that show little interaction across the inter-ring bridge and consequently nearly no energetic separation (*localized* orbitals). The other *n* benzene states of b_1 symmetry result in the *n* energetically largely separated MOs (*delocalized* orbitals). This is exemplified for the case of hexaphenyl in Fig. 2b where the *delocalized* (*localized*) states are denoted by filled (empty) circles. Clearly, the hexaphenyl molecule is of finite length with no translational symmetry, and hence the *Bloch* vector $\boldsymbol{k}$ is not a good quantum number. Nevertheless, one can assign $\boldsymbol{k}$ vectors to the 6 delocalized and 6 localized orbitals leading to the "bands" depicted in Fig. 2b. One can easily imagine, how these states constitute a true band in the limit of an infinitely long chain of phenyl rings (PPP) for which translational symmetry is present and hence the *Bloch* vector $\boldsymbol{k}$ becomes a good quantum number. Only recently, the band structure could be measured on highly-oriented *6P* films by angular-resolved photoemission experiments, confirming this theoretical picture [49].

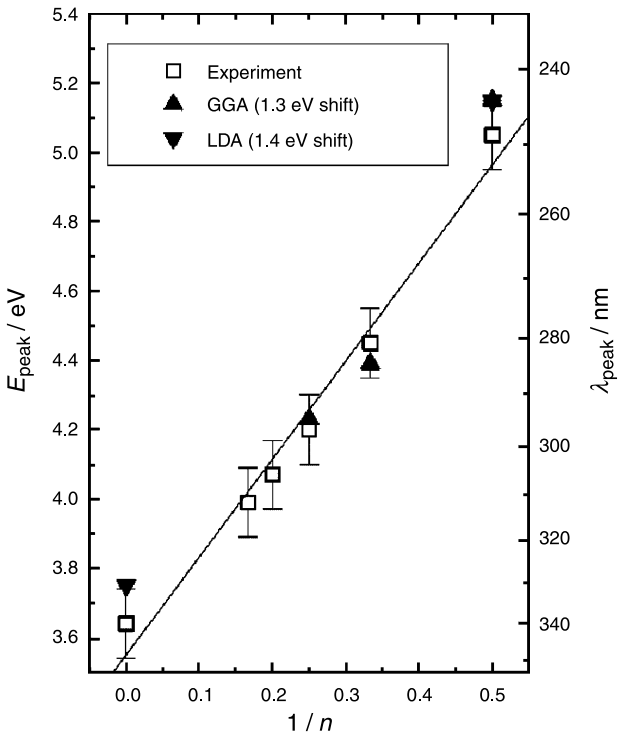

Fig. 3 Position of the first absorption peak as a function of the chain length, where *n* denotes the number of phenyl rings per molecule. Experimental values are taken from Ref. [54]

In a similar manner as described for the highest occupied π-orbitals one can also understand the lowest unoccupied π-states as resulting from the MOs of the benzene ring. Again, this gives rise to a delocalized band with a large, and a localized band with a small band width. Therefore, one can expect the band gap to decrease with increasing molecular length since both, the band widths of the occupied and unoccupied delocalized bands, increase. Experimentally, the band gap follows the so-called $1/n$ law, *i.e.*, the position of the first absorption peak shows a linear dependence as a function of the inverse chain length. This trend is excellently reproduced by the DFT calculations as shown in Fig. 3. Including a scissors shift, independent of the molecular size, the theoretical values lie within the experimental uncertainty which is due to the difference between absorption onset and maximum [50].

Intermolecular interactions

When constructing a molecular crystal from the oligo-phenylene molecules according to the monoclinic crystal structure depicted in Fig. 1 the electronic states of the isolated molecules as discussed in the previous section are modified due to the intermolecular interactions. Since there are two molecules per unit cell each molecular orbital will be split into two states where the splitting is a measure for the intermolecular interaction. Moreover, due to the 3D periodic structure with the lattice vectors $\boldsymbol{a}$, $\boldsymbol{b}$, and $\boldsymbol{c}$, the *Bloch* vector is a good quantum number and we can express the electronic structure of the molecular crystals as a band structure plot for the first Brillouin zone resulting from the direct lattice vectors $\boldsymbol{a}$, $\boldsymbol{b}$, and $\boldsymbol{c}$. The band structures of *2P*, *3P*, *4P*, and *6P* molecular crystals are depicted in Fig. 4.

We start with a description of the electronic bands of biphenyl. As mentioned above, the number of molecular orbitals as depicted in Fig. 2a are doubled in the crystal on account of the herring-bone structure which has two molecules per unit cell. Therefore, the eight top valence bands of crystalline biphenyl clearly resemble the molecular orbital picture. The two highest valence bands (VB) originate from the $2b_{2g}$ MO of the biphenyl molecule. The next four lower lying bands are derived from the $1a_u$ and $1b_{1g}$ states, respectively, whereas VB-6 and VB-7 evolve from the MO of $2b_{3u}$ symmetry. It is interesting to note that the band splittings due to

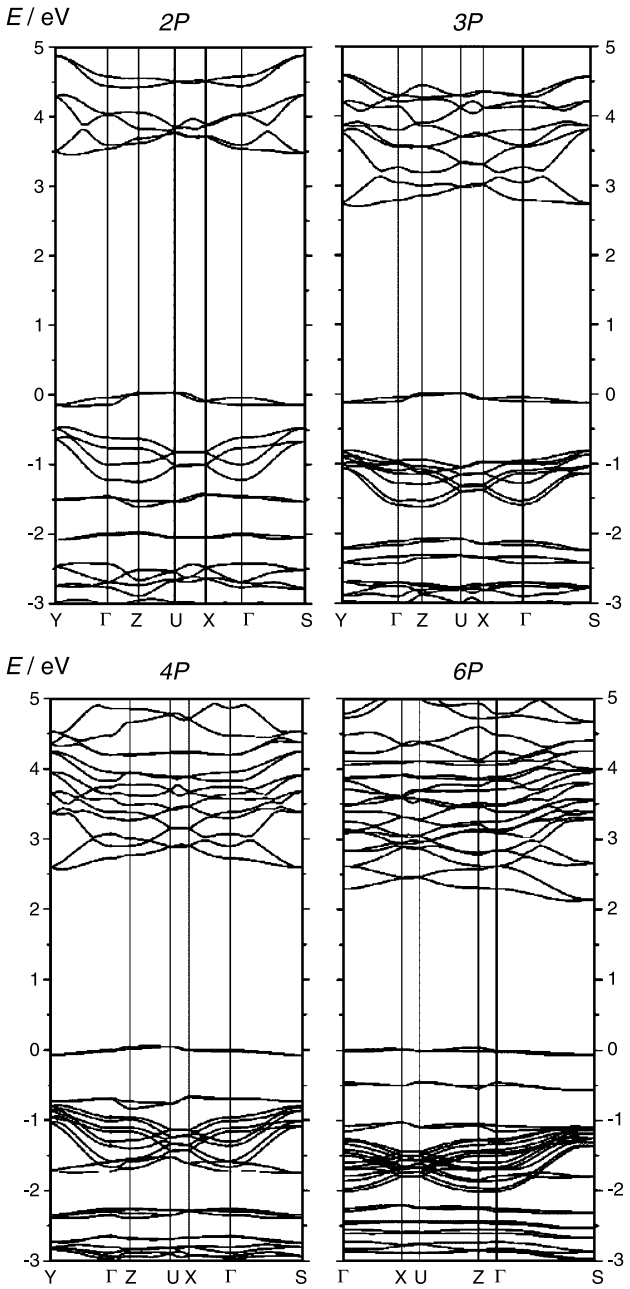

Fig. 4 Electronic band structures of biphenyl (top left), terphenyl (top right), quaterphenyl (bottom left), and hexaphenyl (bottom right). The Fermi level has been set to 0 eV

intermolecular interactions are much larger for the $1a_u$ and $1b_{1g}$ symmetry bands (splitting of more than 0.4 eV at the Γ point), while the interaction is much smaller (splitting of roughly 0.08 eV at Γ) for the $2b_{2g}$ and $2b_{3u}$ bands. In other words, the π-states that are *delocalized* over one oligo-phenylene molecule have little intermolecular interaction, while the π-states that are *localized* on each phenyl ring show

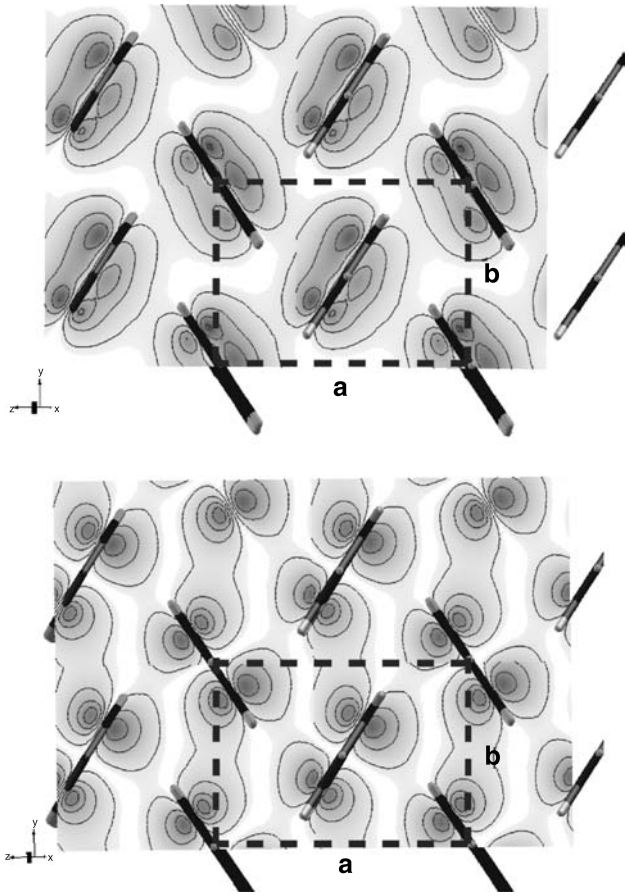

Fig. 5 Contour plot of the wave function in a plane parallel to the *ab* crystal plane of a delocalized (top) and a localized (bottom) π-state. The herring bone arrangement of the molecules is indicated

considerable intermolecular overlap. This is demonstrated in Fig. 5 where we depict the wave functions in a plane parallel to the *ab* crystal plane for a *delocalized* (top panel) and *localized* (bottom panel) state. Clearly, one observes a stronger intermolecular overlap of the wave function for the latter case giving rise to the large intermolecular band dispersion.

Optical properties

The independent particle picture

Within the random phase approximation, *i.e.*, the independent electron-hole picture, the dielectric function is computed from the electronic band structures by summing over all vertical transitions weighted by the optical transition matrix elements. Due to the monoclinic crystal symmetry the dielectric tensor has four independent components, namely

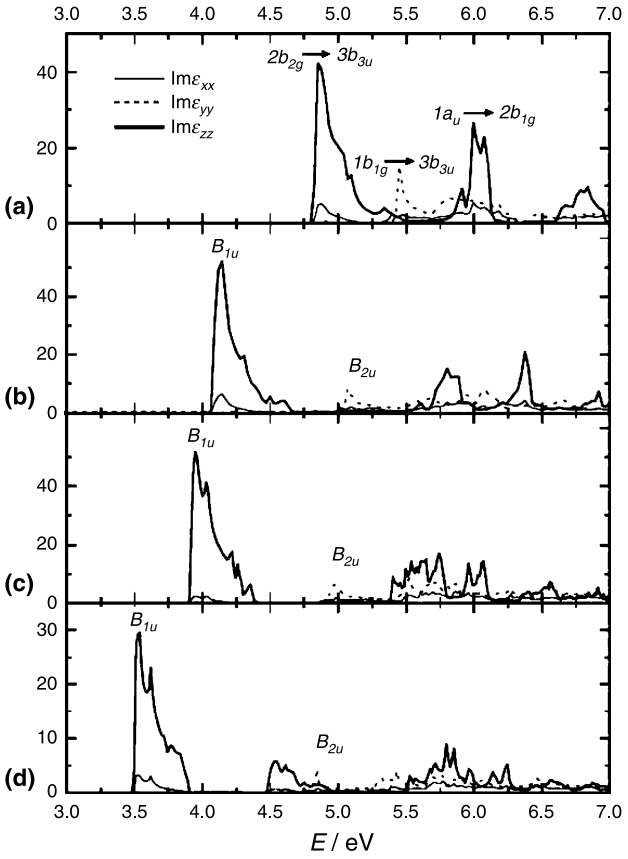

Fig. 6 The imaginary part of the *DF* for *2P* (a), *3P* (b), *4P* (c), and *6P* (d), respectively. The three diagonal components Im ε_{xx}, Imε_{yy} and Imε_{zz} of the dielectric tensors are displayed. The results include a shift of $\Delta_c = 1.3$ eV accounting for the self-energy of the conduction bands. The symmetry of the main transitions is indicated in the MO notation as explained in the text

the diagonal terms *xx*, *yy*, *zz*, and only one off-diagonal component *xz*. The imaginary part of the three diagonal terms for the 2-, 3-, 4-, and 6-unit oligomer is depicted in Fig. 6. The results include a rigid upward shift $\Delta_c = 1.3$ eV accounting for the self-energy correction of the conduction bands.

Similar to the procedure in the previous section, we discuss first, what type of optical excitations and polarizations we have to expect for an isolated biphenyl molecule and compare these qualitative considerations with the *ab initio* results for crystalline biphenyl. As depicted in Fig. 1, we have defined the long molecular axis as the *z*-axis, and the axis perpendicular to *z* and in the plane of the molecule as the *y*-axis. Then, the dipole operator accounting for a polarization parallel to the *z*(*y*)-axis belongs to the B_{1u} (B_{2u}) irreducible representation of D_{2h}. Hence, transitions between two delocalized or between two localized states are polarized in the *z*-direction, whereas transitions between localized and delocalized levels are allowed for polarizations along the *y*-direction. Transitions belonging to the B_{3g} and A_g representation are electric-dipole forbidden by symmetry. Therefore, in an isolated biphenyl molecule, the HOMO to LUMO transition is polarized parallel to the long molecular axis. In the crystal, the polarization of the lowest energy transition remains almost the same and hence the *yy* component is small. The ratio of the *zz* to *xx* component is related to the angle between the molecular axis and the long unit cell axis (compare Fig. 1). At about 0.6 eV above the HOMO-LUMO transition the first ''delocalized-to-localized transitions'' appear. They set up the major part to the *xx* and *yy* component at this energy, but have almost no contribution to *zz*. Excitations that are electric-dipole forbidden in the molecule (B_{3g} and A_g), become weakly allowed in the crystalline environment.

The dielectric functions of *3P*, *4P*, and *6P* are similar to the *DF* of biphenyl. According to the $1/n$ law the lowest transition is red shifted. With increasing oligomer length, the first transition polarized perpendicular to the molecular axis shifts to higher energies with respect to the lowest transition. The peaks in the *yy* component of the *DF* are located 0.6, 0.9, 1.0, and 1.2 eV above the absorption onset in *2P*, *3P*, *4P*, and *6P*, respectively, and their weights decrease with increasing molecular length.

Optical absorption of thin films

In order to be able to compare the theoretical results for the *DF* directly to experimental data it is necessary to calculate optical absorption, transmission, and reflection coefficients of samples consisting of a substrate and a thin film of the organic material. This is achieved by first calculating the real part of the *DF* from the imaginary part *via* the *Kramers-Kronig* relation and, in a second step, applying *Maxwell*'s equations to the layered structures composed of optically anisotropic media [51–53].

The right column of Fig. 7 shows the measured absorbance of a 200 nm thick oriented film of *para*-hexaphenyl (*6P*) [54, 55] together with the theoretical result. The long molecular axis is oriented parallel to the substrate surface. We notice a pronounced dependence of the optical absorption on the polarization of the incoming light. There is a strong

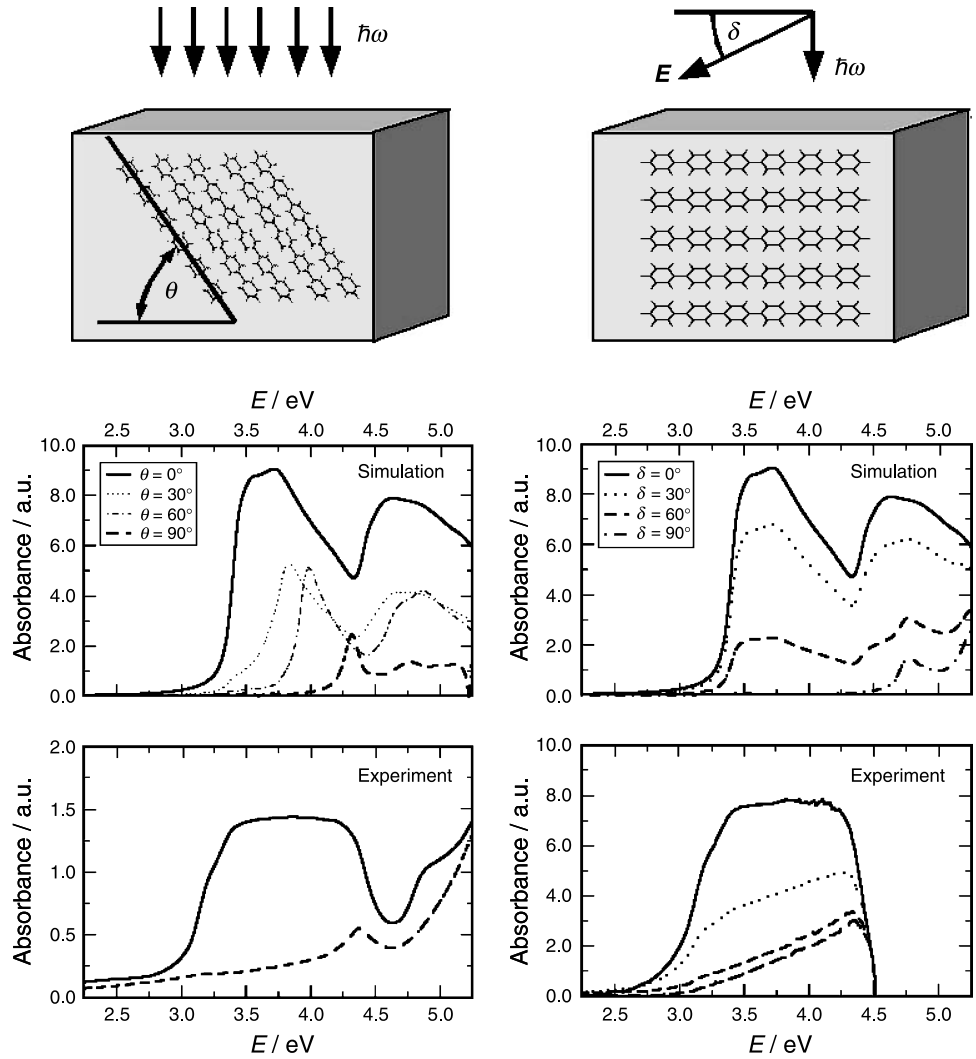

Fig. 7 Left column: Simulated and experimental [53, 54] absorbance of a *para*-hexaphenyl film at normal incidence where the orientation of the molecular axis is varied from *lying* molecules ($\theta = 0°$) to *standing* molecules ($\theta = 90°$). Right column: Simulated and experimental [53, 54] absorbance of an oriented *lying para*-hexaphenyl film where the molecular axis is oriented parallel to the substrate surface. The polarization of the incident light (***E***) is varied from parallel ($\delta = 0°$) to perpendicular ($\delta = 90°$) with respect to the long molecular axis

absorption in the energy range between 3.0 and 4.5 eV when the polarization is parallel to the molecular axis ($\delta = 0°$). Microscopically, the absorption in this energy range is due to the *delocalized* π–π transitions which are optically active for the electric field vector parallel to the molecular axis. For light polarized perpendicular to the chain direction, these transitions can not be excited and the absorbance remains small in the respective energy range. At intermediate polarizations ($\delta = 30°$ and $60°$), the absorption spectra are linear combinations of the curves for parallel and perpendicular polarization, therefore leaving the peak positions unchanged and simply altering the peak intensities. Note that the experimental spectra have only been recorded up to an energy of about 4.2 eV.

One can also study the influence of different molecular orientations within the film which can be achieved by tuning the growth conditions during film preparation or varying the substrate. For instance, the left column of Fig. 7 shows two experimental absorption spectra for two different *6P* films of 200 nm thickness which have been prepared such that (i) the molecules are aligned perpendicular to the substrate, thus the molecules are *standing* on the substrate and (ii), the long molecular axis is parallel to the sub-

strate surface, *i.e.*, the molecules are *lying* flat on the substrate. We compare these two experimental situations with the simulated results by rotating the molecules from their *standing* configuration, characterized by $\theta = 90^\circ$ to the *lying* configuration ($\theta = 0^\circ$) where the molecular axis is parallel to the substrate. We observe a shift of the absorption peak to lower energies and an increase in intensity when the orientation of the molecules is varied from the *standing* to the *lying* configuration. For the two limiting cases, $\theta = 0^\circ$ and 90°, where experiments are available, the agreement is good.

Excitonic effects

Unlike to the situation in *inorganic* semiconductors, like Si or GaAs, where exciton binding energies are found to be small compared to the thermal energy at room temperatures, one expects the electron–hole (e–h) interaction in *organic* semiconductors to be more pronounced. This is due to the strong anisotropies leading to a less effective screening of the e–h interaction, *i.e.*, lower dielectric constants in the latter. In order to develop a quantitative understanding of the optical properties beyond the independent e–h picture as presented in the previous section, it is desirable to devise an *ab initio* approach including excitonic effects. Such an approach is provided within the framework of many-body perturbation theory. Therein, the linear response to an optical perturbation is expressed in terms of the equation of motion for the e–h two-particle Green function, the so-called *Bethe-Salpeter* equation (*BS*E). Solutions of the *BS*E in an *ab initio* framework, appearing in the literature in the past few years, have shown that e–h interactions are indeed important in order to correctly account for quantitative as well as qualitative features of optical spectra of semiconductors and insulators, *i.e.*, a redistribution of oscillator strengths as well as bound excitons. This is true for inorganic as well as for organic semiconductors as discussed in the reviews, Refs. [39] and [40]. The implementation of the *BS*E method into the LAPW method has been published in Ref. [56].

The exciton binding energy (*BE*) is a central quantity in the photophysics of organic semiconductors since it is intimately related to the probability of radiative emission/absorption and electric-field induced generation of free charge carriers. The *BE* is defined as the energy required to separate a bound

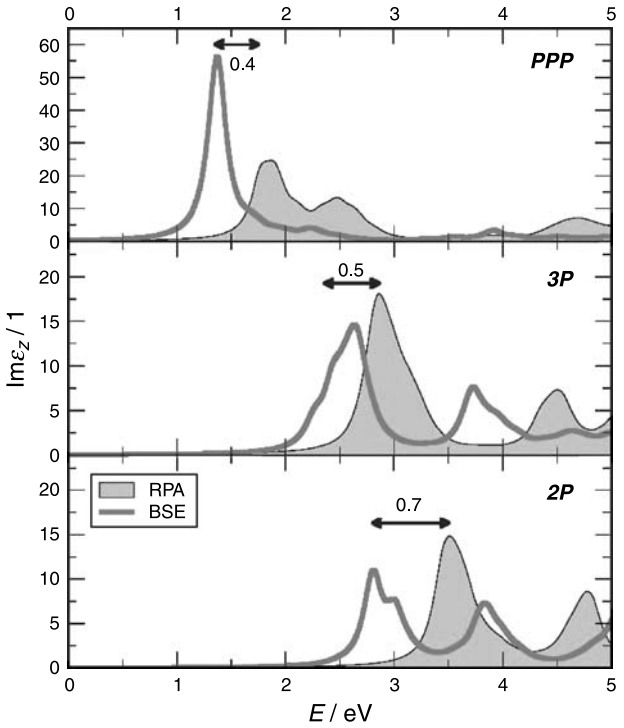

Fig. 8 The imaginary part of the macroscopic dielectric tensor *zz*-component for the phenylenes (*PPP* to *2P* from top to bottom). Independent electron-hole spectra (shaded areas) are compared to *BS*E spectra including excitonic effects and the exciton binding energies of the lowest singlet states are indicated

e–h pair, the exciton, into a free electron and a free hole. The solution of the *BS*E could indeed clarify the nature of the energetically lowest optical excitations in these organic semiconductors, and hence close the longstanding debate whether the lowest energy transitions are due to weakly bound *Wannier* excitons (or even independent charge carriers) or due to the absorption of tightly bound excitons (*Frenkel* exciton model).

In Fig. 8, we investigate how the exciton binding energy depends on the length of the molecular building blocks going from biphenyl to the infinite polymer chain. The imaginary part of the macroscopic dielectric tensor is depicted for *2P*, *3P*, and *PPP*. A common feature, not only observed for the phenylenes but also for the acenes [57, 58] and thiophenes [40], is the reduction of the exciton binding energy with increasing molecular length. This is a consequence of the decreasing e–h *Coulomb* interaction, when the molecular size increases, which can be attributed to two effects: (i) a larger extension of the e–h wave function and (ii) the strong enhancement of the dielectric screening. While the latter is a

result of the previously discussed reduction of the electronic band gap with increasing molecular length, the former can be explained by spatially more extended e–h clouds along the molecular backbone allowing for a larger separation of the electron and the hole, when the length of the molecule increases.

Conclusions and outlook

We have shown how *ab initio* DFT calculations contribute to an understanding of the electronic and optical properties of the organic semiconducting materials which form the active layers in many electro-optical applications. These investigations revealed important structure-property relations and can provide guidelines for the optimization of devices based on these organic semiconductors. Thus, the first-principles investigations presented in this review focused on the *intrinsic* electronic and optical properties of the active organic layers. The operation of a device like an OLED or an OFET is, however, also crucially determined by the interface between a metal electrode and the organic semiconductor. For instance, the charge carrier injection from the electrode into the organic material depends on the alignment of the electronic levels. Moreover, the interactions between the organic molecule and the metal surface determines the molecular order at the interface and the film growth. Therefore, future investigations have to be directed to an understanding of the interfaces of organic semiconductors with metal surfaces or other (organic) semiconductors. To this end, it will be important to extend the current theoretical approach by an *ab initio* treatment of *van der Waals* interactions as recently developed by *Dion et al.* [59]. First results for surface energies [60] and the adsorption of thiophene on Cu(110) [61] indeed highlight the importance of this nonlocal correlation effect.

Acknowledgements

A number of people have contributed to the work presented in this review, namely *K. Hummer* and *S. Sagmeister* from the authors' group, and, in addition, several colleagues from the Graz University of Technology providing us with valuable experimental data, *G. Heimel*, *M. Oehzelt*, *R. Resel*, and *E. Zojer*. The work was financially supported by the FWF, projects P16227 and S9714. The latter is part of the joint experimental/theoretical National Research Network Interface Controlled and Functionalized Organic Films.

References

1. Tang CW, VanSlyke SA (1987) Appl Phys Lett 51:913
2. Burroughes JH, Bradley DDC, Brown AR, Marks RN, McKay K, Friend R, Burns PL, Holmes AB (1990) Nature 347:539
3. Friend R, Gymer RW, Holmes AB, Burroughes JH, Marks RN, Taliani C, Bradley DDC, Dos Santos DA, Bredas JL, Logdlund M, Salaneck WR (1999) Nature 397:121
4. Dimitrakopoulos CD, Mascaro DJ (2001) IBM J Res Dev 45:11
5. Sariciftci NS, Smilowitz L, Heeger AJ, Wudl F (1992) Science 258:1474
6. Granström M, Petritsch K, Arias AC, Lux A, Andersson MR, Friend RH (1998) Nature 395:257
7. Brabec CJ, Sariciftci NS, Hummelen JC (2001) Adv Funct Mater 11:15
8. Polson RC, Vardeny ZV (2005) Phys Rev B 71:45205
9. Strangi G, Barna V, Caputo R, Luca AD, Versace C, Scaramuzza N, Umeton C, Bartolino R, Price GN (2005) Phys Rev Lett 94:63903
10. Heeger AJ (2002) Synth Met 125:23
11. Kim D, Cho H, Kim CY (2000) Prog Polym Sci 25:1089
12. Era M, Tsutsui T, Saito S (1995) Appl Phys Lett 67:2436
13. Torsi L, Dodabalapur A, Rothberg LJ, Fung AWP, Katz HE (1996) Science 272:1462
14. Dimitrakopoulos CD, Brown AR, Pomp A (1996) J Appl Phys 80:2501
15. Nelson S, Lin YY, Gundlach DJ, Jackson TN (1998) Appl Phys Lett 72:1854
16. Horowitz G (1998) Adv Mater 10:365
17. Pope M, Swenberg CE (1999) Electronic Processes in Organic Crystals and Polymers. Oxford University Press, New York, USA
18. Silinsh EA (1980) Organic Molecular Crystals. Springer-Verlag, Berlin Heidelberg New York Germany
19. Cornil J, Beljonne D, Bredas JL (1995) J Chem Phys 103:834
20. Bredas JL (1997) Synth Met 84:3
21. Cheng YC, Silbey RJ, da Silva Filho DA, Calbert JP, Cornil J, Bredas JL (2003) J Chem Phys 118:3764
22. Tiago ML, Northrup JE, Louie SG (2003) Phys Rev B 67:115212
23. Hummer K, Puschnig P, Ambrosch-Draxl C (2003) Phys Rev B 67:184105
24. Hummer K, Ambrosch-Draxl C (2005) Phys Rev B 72:205205
25. Endres RG, Fong CY, Yang LH, Witte G, Wöll C (2004) Comp Mat Sci 29:362
26. Ambrosch-Draxl C, Majewski JA, Vogl P, Leising G (1995) Phys Rev B 51:9668
27. Puschnig P, Ambrosch-Draxl C (1999) Phys Rev B 60:7891
28. Puschnig P, Hummer K, Ambrosch-Draxl C, Heimel G, Oehzelt M, Resel R (2003) Phys Rev B 67:235321
29. Ferretti A, Ruini A, Molinari E, Caldas MJ (2003) Phys Rev Lett 90:86401
30. Hohenberg P, Kohn W (1964) Phys Rev 136:B864

31. Kohn W, Sham LJ (1965) Phys Rev 140:A1133
32. Jones RO, Gunnarsson O (1989) Rev Mod Phys 61:689
33. Kohn W (1999) Rev Mod Phys 71:1253
34. Perdew JP, Burke K, Ernzerhof M (1996) Phys Rev Lett 77:3865
35. Adler SL (1962) Phys Rev 126:413
36. Wiser N (1963) Phys Rev 129:62
37. Del Sole R, Girlanda R (1993) Phys Rev B 48:11789
38. Ambrosch-Draxl C, Sofo JO (2006) Comp Phys Commun 175:1
39. Onida G, Reining L, Rubio A (2002) Rev Mod Phys 74:601
40. Hummer K, Puschnig P, Sagmeister S, Ambrosch-Draxl C (2006) Mod Phys Lett B 20:261
41. Blaha P, Schwarz K, Madsen GKH, Kvasnicka D, Luitz J (2001) WIEN2k, Vienna University of Technology, Vienna
42. Baudour JL (1991) Acta Crystallogr 47:935
43. Zojer E, Cornil J, Leising G, Bredas JL (1999) Phys Rev B 59:7957
44. Baudour JL, Cailleau H, Yelon WB (1977) Acta Crystallogr 33:1773
45. Charbonneau GP, Delugeard Y (1977) Acta Crystallogr 33:1586
46. Rietveld HM, Maslen EN, Clews CJB (1970) Acta Crystallogr 26:693
47. Delugeard Y, Desuche J, Baudour JL (1976) Acta Crystallogr 32:702
48. Baker KN, Fratini AV, Resch T, Knachel HC, Adams WW, Socci EP, Farmer BL (1993) Polym Papers 34:1571
49. Koller G, Berkebile S, Oehzelt M, Puschnig P, Ambrosch-Draxl C, Netzer FP, Ramsey MG (2007) Science 317:351
50. Ambrosch-Draxl C, Puschnig P, Resel R, Leising G (1999) Synth Met 101:673
51. Yeh P (1980) Surf Sci 96:41
52. Mansuripur M (1990) J Appl Phys 67:6466
53. Puschnig P, Ambrosch-Draxl C (2006) Adv Eng Mat 8:1151
54. Niko A, Meghdadi F, Ambrosch-Draxl C, Vogl P, Leising G (1996) Synth Met 76:177
55. Zojer E, Koch N, Puschnig P, Meghdadi F, Niko A, Resel R, Ambrosch-Draxl C, Knupfer M, Fink J, Bredas JL (2000) Phys Rev B 61:16538
56. Puschnig P, Ambrosch-Draxl C (2002) Phys Rev B 66:165105
57. Hummer K, Puschnig P, Ambrosch-Draxl C (2004) Phys Rev Lett 92:147402
58. Hummer K, Ambrosch-Draxl C (2005) Phys Rev B 71:081202(R)
59. Dion M, Rydberg H, Schröder E, Langreth DC, Lundquist BI (2004) Phys Rev Lett 92:24601
60. Nabok D, Puschnig P, Ambrosch-Draxl C (to be published)
61. Sony P, Puschnig P, Nabok D, Ambrosch-Draxl C. Phys Rev Lett (accepted)